

Orthogonal-Port Isolation in Wide-Scan Triangular-Lattice Dual-Polarized mmWave Arrays Using Unbalanced-Fed Patch Antennas

Downloaded from: https://research.chalmers.se, 2026-11-23 19:40 UTC

Citation for the original published paper (version of record):
Pavlidis, T., Vilenskiy, A., Schäfer, T. et al (2026). Orthogonal-Port Isolation in Wide-Scan Triangular-Lattice Dual-Polarized mmWave Arrays Using Unbalanced-Fed Patch Antennas. 2026 56th European Microwave Conference (EuMC). http://dx.doi.org/10.23919/EuMC69230.2026.11748330

N.B. When citing this work, cite the original published paper.

research.chalmers.se offers the possibility of retrieving research publications produced at Chalmers University of Technology. It covers all kind of research output: articles, dissertations, conference papers, reports etc. since 2004. research.chalmers.se is administrated and maintained by Chalmers Library

(article starts on next page)

Orthogonal-Port Isolation in Wide-Scan Triangular-Lattice Dual-Polarized mmWave Arrays Using Unbalanced-Fed Patch Antennas

Theodoros Pavlidis[#1], Artem R. Vilenskiy[^], Thomas Schäfer[$], Ahmed A. Kishk[*], and Marianna V. Ivashina[#2]

[#]Antenna Systems Group, Dept. of Electrical Engineering, Chalmers University of Technology, Gothenburg, Sweden

[^]XPANCEO, Dubai, UAE

[$]Satcube AB, Gothenburg, Sweden

[*]Concordia University, Montreal, QC H3G 1M8, Canada

{[1]pavlidis, [2]marianna.ivashina}@chalmers.se

***Abstract*— Triangular lattices (TLs) are attractive for wide-scan phased arrays because they increase the unit cell (UC) area by about 15.5% compared with rectangular lattices (RELs). However, several studies on dual-polarized (DP) arrays have reported degraded orthogonal port isolation in TLs. This paper compares the isolation performance of unbalanced-fed, wide-scan ($\theta_s \leq 60°$) DP patch arrays in equilateral TLs and RELs with element spacings $\lambda_0/\sqrt{3}$ and $\lambda_0/2$, respectively. First, the isolation-versus-scan behavior is examined across frequency, showing that approaching grating-lobe onset degrades isolation. Then, both non-slant (aligned with the lattice axes) and slant UC layouts ($45°$-rotated) are evaluated. For the studied topology, the TL maintains isolation performance comparable to that of the REL. The results indicate that the isolation degradation often reported for TLs is not universal, and that low-profile, DP patch arrays can exploit the TL while preserving wide-scan isolation.**

***Keywords*— phased arrays, microstrip antenna arrays, triangular lattice.**

I. Introduction

Wide-scanning phased array antennas (PAAs) impose stringent constraints on RF front-end integration, packaging, and thermal management due to the inherently tight element spacing. These challenges are further exacerbated by dual-polarized (DP) operation, which doubles the number of RF front-end channels. At millimeter-wave (mmWave) frequencies, the need for a small inter-element spacing to suppress grating lobes further reduces the available area per element, making routing, thermal dissipation, and electronic integration particularly challenging.

A way to increase the element area is to adopt a triangular lattice (TL) architecture. Particularly interesting is the equilateral TL, which enables a symmetrical scan region (grating lobes first appear for the same θ_s). The equilateral TL yields an element area that is increased by a factor of $2/\sqrt{3}$ (approximately 15.5%) compared to a rectangular lattice (REL) for the same continuous 2-D scan criterion [1]. However, the TL features a element arrangement and therefore mutual coupling environment, which can modify the antenna performance observed in a REL.

Several researchers have benchmarked arrays realized in RELs and TLs. Some studies compared the onset of scan blindness [2] and scan bandwidth [3] of dipole arrays in the two lattices. However, they were limited to a single polarization and did not address introducing a second polarization. Other researchers compared DP arrays in TLs and RELs. These include Vivaldi arrays [4], [5], arrays of additively manufactured dipoles [6], arrays of interconnected rings [7], planar ultrawideband modular arrays (PUMAs) [8], as well as waveguide arrays [9]. However, for many PAA applications, the microstrip patch element is the preferred solution due to the ease of fabrication, low profile and integration potential. While there are numerous examples of wide-scanning, DP patch PAAs in TLs [10], [11], [12], [13], [14], [15], to the best of the authors' knowledge, no study in the open literature investigates the performance tradeoffs of using TLs or RELs for DP PAAs of patch elements.

An important tradeoff observed in several performance comparison studies of DP arrays in RELs and TLs is a reduction of orthogonal port isolation in TLs [4], [6], [8], [7], which has been attributed to the reduced symmetries of DP PAs when arranged in TLs. This effect is aggravated near the upper frequency limit [8], [13] by the decreased attenuation of higher-order Floquet modes (grating lobes), that provide additional pathways for orthogonal port coupling. Modal attenuation can be increased by reducing element spacing [16], but this diminishes the benefits of using a TL.

Several solutions have been proposed to improve orthogonal port isolation in TLs. In [11], feed rotation is implemented to improve the isolation of a probe-fed patch PAA. However, the improvements in isolation resulting from the feed rotation are not quantified. An array of tri-ridge waveguides is demonstrated in [17], achieving $>$ 15 dB isolation in two ϕ_s-planes for $\theta_s \leq 60°$ by co-locating $\lambda_0/4$ decoupling corrugations with orthomode transducers (OMTs) for dual-polarization. Unfortunately, both structures increase the array's profile. Alternatively, differential feeding can provide high isolation. Baluns for wide-scanning mmWave PAs have been proposed [18], [19], but require additional conductor layers and increase losses.

This work addresses both the lack of comparative studies of DP wide-scanning patch PAAs in RELs and TLs, and

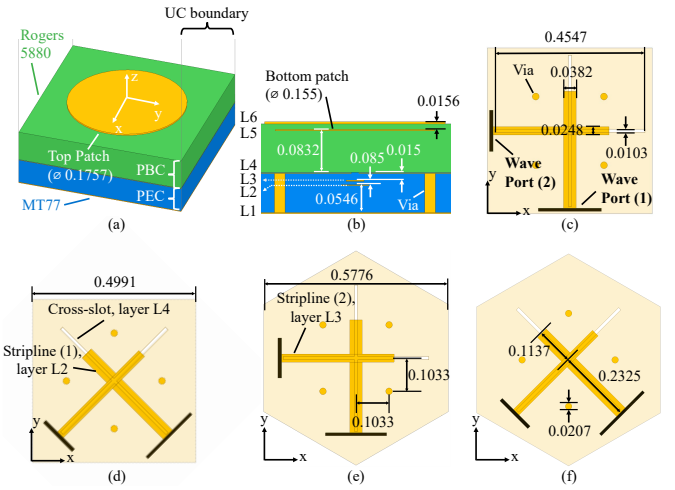


Fig. 1. UC geometries (a) 3-D view, REL, (b) PCB cross-section. L2-L4 layers of (c) non-slant REL, (d) slant REL, (e) non-slant TL, and (f) slant TL. Dimensions are given as a function of λ_0, which is the free space wavelength at f_0. Conductor thicknesses are $0.0043\lambda_0$ and $0.0019\lambda_0$ for L6 and L1-L5, respectively. The dimensions not noted in various UCs are identical to the equivalent of other UCs and/or symmetrical to those of the orthogonal polarization.

the open question of whether the orthogonal port isolation degradation often reported for TLs is intrinsic, or instead topology-dependent and therefore avoidable in unbalanced-fed patch arrays. To this end, the isolation-versus-scan behavior of cross-slot-fed [20] patch PAA unit cells (UCs) with different lattice configurations is investigated. The rest of the paper is organized as follows: in Sec. II, the performance of the cross-slot fed patch PAAs in RELs and TLs is examined, and the TL results are compared with the state-of-the-art. Conclusions are drawn in Sec. III.

II. Performance Comparison

The investigated UC architectures are depicted in Fig. 1. Each UC utilizes a 6-layer PCB [Fig. 1(b)], with the stripline feeds and their ground planes placed in Astra MT77 substrate ($\varepsilon_r = 3$, $\tan\delta = 0.0017$) while the microstrip patches are etched on Rogers 5880 laminate ($\varepsilon_r = 2.2$, $\tan\delta = 0.0009$). The two striplines on layers L2 and L3 excite a cross-slot aperture on L4. A PEC boundary condition surrounds the UC boundaries from L1 to L4 to stop the propagation of parallel-plate-waveguide (PPW) modes between the stripline ground planes (L1 and L4). The PEC boundary condition can be approximated by closely-spaced metallic vias in practical implementations. Four L1-L4 vias are used to suppress resonances of the cavity formed by the PEC walls and the ground planes. The cross-slot feeds the stacked patches on L5 and L6. The TL UCs (see Figs. 1(e) and (f)) have a hexagonal shape to facilitate dual-polarization design. The slant UCs (shown in Figs. 1(d) and (f)) are obtained by rotating the striplines, the wave ports, the slots, and the vias of the non-slant UCs by $\phi = 45°$. The dimensions of these components remain constant between the UCs. The UC spacing is approximately $\lambda_0/2$ and $\lambda_0/\sqrt{3}$ for the REL and TL UCs, respectively, enabling grating lobe-free scanning at

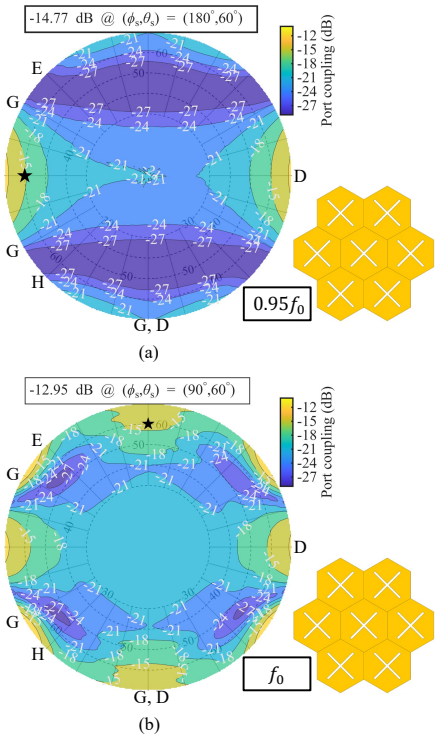


Fig. 2. Orthogonal port coupling (to port 2 when port 1 is excited) for $\theta_s \leq 70°$ in a 2-D infinite array environment for (a) $0.95f_0$, and (b) f_0. Noted above the contour maps are the maximum orthogonal port coupling values for $\theta_s \leq 60°$ and the scan angle of occurrence. E - port 1 E-plane, H - port 1 H-plane, D - D-plane, G - plane where grating lobes first radiate with increasing frequency. In each subfigure, an array fragment consisting of the L6 layer of a center UC and its neighboring UCs is depicted.

f_0 for $\theta_s \leq 90°$ in both cases. To model the conductor layer and via copper surface roughness in the Ka-band, the Huray model with a nodule radius of 0.7 μm and a surface ratio of 3.8 is used. In Ansys HFSS, periodic boundary conditions (PBCs) are enforced on the UC sidewalls above L4, and the space above the aperture is terminated with a Floquet port to simulate an infinite array. For all UCs, $|\Gamma_{act}| < -10$ dB for both ports at broadside.

First, to highlight that approaching the onset of grating lobes can increase port coupling, we compare port coupling in Fig. 2 for the slant TL at f_0 and $f' = 0.95f_0$. At $f' = 0.95f_0$ [Fig. 2(a)], the scan angles with isolation < 15 dB are limited to the areas around the D-plane with $\phi_s = 0°$ and $\phi_s = 180°$. On the other hand, as can be seen in Fig. 2(b), additional areas of < 15 dB isolation appear at f_0 on the planes where grating lobes first radiate with increasing frequency. Similarly, the plane where the minimum isolation is encountered for $\theta_s \leq 60°$ shifts to the D-plane at $\phi_s = 90°$. These results demonstrate that approaching the onset of radiating grating lobes can reduce port isolation.

Then, port isolation versus scan for the UCs depicted in Figs. 1(c)-(f) is compared. The results are shown in Fig. 3. For the non-slant REL UC [Fig. 3(a)], port coupling is maximized along a D-plane direction, as expected from previous studies [6]. For the non-slant TL (see Fig. 3(b)), however, the port coupling maximum is shifted from the D-plane due to a

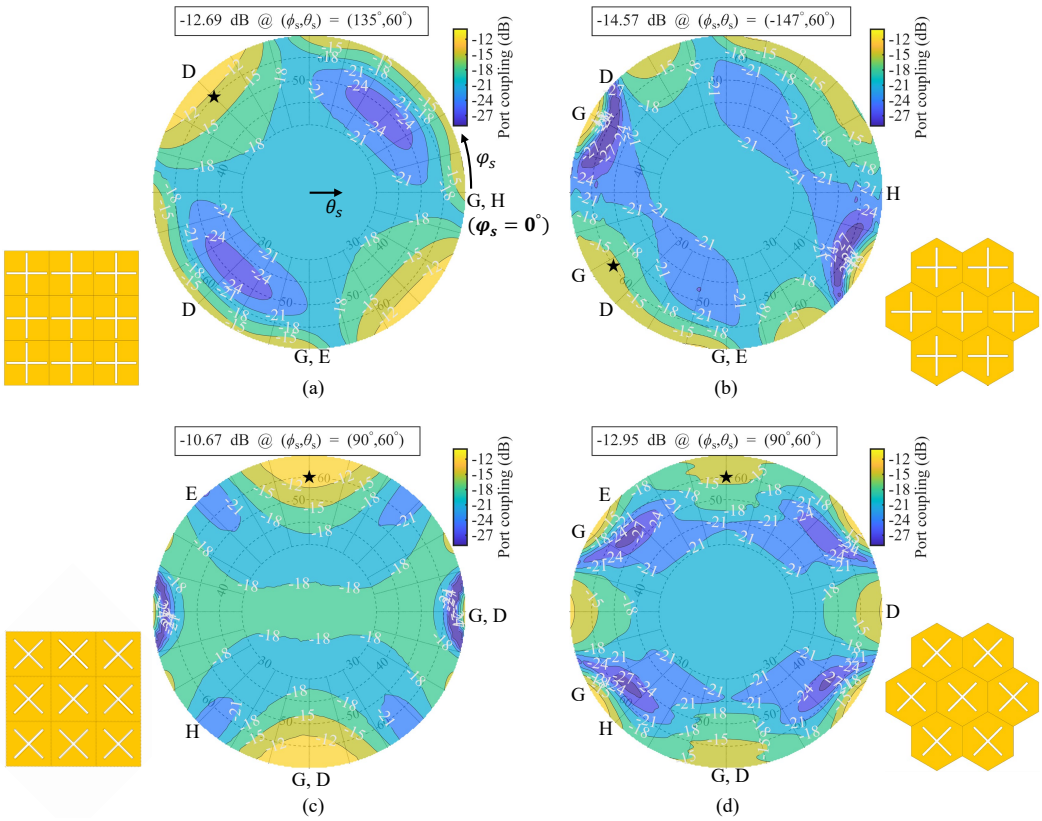


Fig. 3. Orthogonal port coupling (to port 2 when port 1 is excited) at $f = f_0$ for $\theta_s \leq 70°$ in 2-D infinite array environment. (a) Non-slant square REL, (b) non-slant TL, (c) slant REL, and (d) slant TL. Noted above the contour maps are the maximum orthogonal port coupling values for $\theta_s \leq 60°$ and the scan angle of occurrence. E - port 1 E-plane, H - port 1 H-plane, D - D-plane, G - plane where grating lobes first radiate with increasing frequency. In each subfigure, an array fragment consisting of the L6 layer of a center UC and its neighboring UCs is depicted.

grating lobe approaching the visible region. The effect of using slant-polarized UCs is then examined. For the slant REL case [Fig. 3(c)], the port coupling maximum remains in the D-plane. However, it is ~ 2 dB higher than the non-slant REL. Similar results are observed in Fig. 3(d) for the slant TL. It is notable that the minimum isolation for $\theta_s \leq 60°$ remains similar for both lattices, suggesting that the cross-slot-fed patch UC does not suffer from degraded isolation in TL configurations, in contrast to previous works [4], [6], [8], [7]. This result is practically important because, for the studied topology, the TL provides an approximately 15% larger UC area than the REL, while showing no significant degradation in orthogonal port isolation within the considered scan region. This comparable isolation performance can be attributed to two characteristics. First, the UC segment most susceptible to mutual-coupling effects (above layer L4) exhibits two symmetry planes, aligned with the x- and y-axes in Fig. 1(c). Several studies have highlighted the role of symmetry in improving port isolation [21], [22]. Second, the unbalanced feed lines are routed below the patch ground plane, facilitating their decoupling by means of vias.

We compare our results to other DP arrays in a TL in Table 1. To ensure equal grating lobe constraints, we have excluded from the table the PAs presented in [11] and [13]. The patch PAA in [11] operates at frequencies with element spacing $< \lambda_0/\sqrt{3}$. The probe-fed patch PAA in [13], on the other hand, features > 15 dB isolation for $\theta_s \leq 60°$ over 13% bandwidth. However, this isolation value quickly deteriorates to < 7 dB at higher frequencies, and the element spacing is not disclosed, complicating comparisons with this work. The cross-slot fed patch PAA achieves a competitive isolation performance for electrically equal $\lambda_0/\sqrt{3}$ element spacings. Importantly, this value is achieved for continuous 2-D scan, while most other works report 2 or 3 ϕ_s-planes.

Table 1. Comparison of isolation for 2-D $\theta_s \leq 60°$ scanning DP PAAs in equilateral TL for $\lambda_0/\sqrt{3}$ spacing.

Ref.	Element	Profile (λ_0)	No. of ϕ_s-planes	Iso. (dB)
[4]	Vivaldi	3.4	$3^{\text{E, H, D1}}$	13
[5]	Vivaldi	3.46	$3^{\text{E, H, D1}}$	12
[6]	Metal dipole	0.77	$4^{\text{E, H, D2}}$	12
[8]	PUMA	0.52	$3^{\text{E, H, D1}}$	5
[9]	Waveguide	N/A†	4	9.5
[17]	Waveguide	> 0.64*	2	15
T.W	Patch	0.18	Continuous 2-D	12.9

†N/A - not applicable, semi-infinite waveguide assumed. *Not including the OMT height. Ref. - Reference, Iso. - Isolation, E - E-plane scan, H - H-plane scan, D1 - for scanning in one of the D-planes, D2 - for scanning in both D-planes. T.W. - This Work. Refers to slant TL.

III. Conclusion

This paper has presented a performance comparison of DP patch PAA UCs in RELs and TLs under equal grating-lobe constraints. The study showed that orthogonal port isolation deteriorates as the operating frequency approaches grating-lobe onset, confirming the role of higher-order Floquet modes in coupling degradation. It was further shown that, for the investigated cross-slot-fed patch topology, the TL does not introduce the pronounced isolation penalty reported for several other arrays of DP elements, such as Vivaldi, PUMA, and interconnected ring elements. This holds for both the non-slant and the slant layouts. In both cases, the TL achieved isolation performance comparable to that of the REL while preserving its larger UC area.

These results provide a practically important design insight: low-profile, unbalanced-fed DP patch arrays can exploit the relaxed spacing constraints of TLs without sacrificing competitive wide-scan isolation. This makes the TL a viable option for highly integrated mmWave phased arrays, where routing, thermal management, and front-end packaging strongly benefit from increased UC area. Experimental validation of mmWave cross-slot fed patch PAs in TLs has already been demonstrated for the Ka-band in PCB technology [23] - future work will focus on Q- and V-band operation.

Acknowledgment

Funded in part by the Swedish Research Council (VR) through the 6G-NTN-E Research Environment under Grant 2024-06645, and in part by the European Union, under ANTERRA 101072363 HORIZON-MSCA-2021-DN-01. Views and opinions expressed are however those of the author(s) only and do not necessarily reflect those of the European Union. Neither the European Union nor the granting authority can be held responsible for them.

References

[1] E. Sharp, "A triangular arrangement of planar-array elements that reduces the number needed," *IRE Trans. Antennas Propag.*, vol. 9, no. 2, pp. 126–129, 1961.

[2] D. Pozar and D. Schaubert, "Scan blindness in infinite phased arrays of printed dipoles," *IEEE Trans. Antennas Propag.*, vol. 32, no. 6, pp. 602–610, 1984.

[3] C. I. Kolitsidas and B. L. G. Jonsson, "Rectangular vs. equilateral triangular lattice comparison in a T-slot loaded strongly coupled dipole array," in *2014 XXXIth URSI General Assem. Sci. Symp.*, pp. 1–4.

[4] R. W. Kindt and B. T. Binder, "Dual-polarized Vivaldi array on a triangular lattice," *IEEE Trans. Antennas Propag.*, vol. 69, no. 4, pp. 2083–2091, 2021.

[5] C. Pfeiffer, J. Massman, and T. Steffen, "3-D printed metallic dual-polarized Vivaldi arrays on square and triangular lattices," *IEEE Trans. Antennas Propag.*, vol. 69, no. 12, pp. 8325–8334, 2021.

[6] R. W. Kindt and B. T. Binder, "Wideband, low-profile, dual-polarized machined-metal array on a triangular lattice," *IEEE Trans. Antennas Propag.*, vol. 70, no. 2, pp. 1097–1106, 2022.

[7] Y. Zhang, Q. Shi, A. El-Makadema, L. Danoon, and A. K. Brown, "Triangular grid interconnected crossed rings antenna for large-scale ultra-wideband dual-polarised arrays," *IET Microw., Antennas Propag.*, vol. 14, no. 15, pp. 2115–2122, 2020.

[8] R. W. Kindt and B. T. Binder, "Dual-polarized planar-printed ultrawideband antenna array on a triangular grid," *IEEE Trans. Antennas Propag.*, vol. 68, no. 8, pp. 6136–6144, 2020.

[9] C. Vazquez-Sogorb, R. Montoya-Roca, G. Addamo, O. A. Peverini, and G. Virone, "Ridged apertures for LEO direct radiating arrays in Ka-band," *Appl. Sci.*, vol. 14, no. 17, 2024.

[10] P. Gorski, F. Bongard, D. L. del Rio, A. D. Bolado, M. Elsbury, M. Renard, J. Sarmiento, and M. C. Vigano, "Low-cost phased array for land mobile application," in *2025 55th Eur. Microw. Conf.*, pp. 1223–1226.

[11] G. Gültepe, T. Kanar, S. Zihir, and G. M. Rebeiz, "A 1024-element Ku-band SATCOM dual-polarized receiver with >10-dB/K G/T and embedded transmit rejection filter," *IEEE Trans. Microw. Theory Techn.*, vol. 69, no. 7, pp. 3484–3495, 2021.

[12] T. Takahashi, H. Watanabe, Y. Matsuda, K. Takanishi, A. Hirai, K. Yamamoto, T. Okura, and H. Tsuji, "Dual-beam and wide-angle steering AESA with antenna size scalability for Ka-band SATCOM," in *2024 IEEE Int. Symp. Phased Array Syst. Technol.*, 2024, pp. 1–5.

[13] B. Lesur, C. Menudier, and M. Thévenot, "Wide-angle beam steering Ka-band Rx active phased array for satellite communications," in *2024 IEEE Int. Symp. Phased Array Syst. Technol.*, pp. 1–4.

[14] D. Milroy, D. E. Adams, and E. Yetisir, "Antenna apparatus having antenna spacer," U.S. Patent 11509048 B2, 2022.

[15] K. van Hastenberg, G. Theis, M. H. Mazaheri, W. M. Abdel-Wahab, A. Smolders, and U. Johannsen, "A polarisation-agile phased-array antenna for satellite and beyond-5G communications," in *2022 IEEE Int. Symp. Antennas Propag. and USNC-URSI Radio Sci. Meeting*, 2022, pp. 1832–1833.

[16] A. K. Bhattacharyya, "Introduction to Floquet modes in infinite arrays," in *Phased Array Antennas: Floquet Analysis, Synthesis, BFNs, and Active Array Systems*. Hoboken, NJ, USA: Wiley, 2005, ch. 2, pp. 61–87.

[17] L. Polo-López, L. Berretti, E. Menargues, S. Capdevila, G. Toso, and M. García-Vigueras, "Dual-polarized spaceborne phased arrays using tri-ridge evanescent waveguide antennas," *IEEE Antennas Wireless Propag. Lett.*, vol. 24, no. 3, pp. 656–660, 2025.

[18] T. van der Spuy, R. Maaskant, S. E. Gunnarson, H. Holter, and L. Nyström, "Wideband millimeter-wave balun-diplexer based on a novel coupled Marchand architecture for compact footprint and phased-array integration," *Microw. Opt. Technol. Lett.*, vol. 67, no. 11, p. e70460, 2025.

[19] K. Yang, Z. R. He, S. C. Jin, Y. Q. Yang, Y. Fan, and Y. J. Cheng, "K-/Ka-band dual-CP planar shared-aperture wide-angle scanning array antenna with embedded diplexer and cancellation network for >45-dB Tx–Rx isolation," *IEEE Trans. Antennas Propag.*, vol. 74, no. 2, pp. 1591–1600, 2026.

[20] Y. Zhang, S. Ogurtsov, V. Vasilev, A. R. Vilenskiy, A. A. Kishk, M. V. Ivashina, and D. Caratelli, "Dual-polarized dielectric-filled cavity antenna with air-gap-free metasurface loading for LTCC-based 5G-and-beyond antenna-in-package phased arrays," *IEEE Trans. Antennas Propag.*, vol. 74, no. 2, pp. 1293–1307, 2026.

[21] E. Shepeleva, A. Vilenskiy, G. Evtyushkin, and A. Lukyanov, "Sub-THz U-slot coupled stacked-patch radiating elements for dual-polarized MIMO array antennas," in *2024 18th Eur. Conf. Antennas Propag.*, pp. 1–5.

[22] M. Mirmozafari, G. Zhang, C. Fulton, and R. J. Doviak, "Dual-polarization antennas with high isolation and polarization purity: A review and comparison of cross-coupling mechanisms," *IEEE Antennas Propag. Mag.*, vol. 61, no. 1, pp. 50–63, 2019.

[23] T. Pavlidis, T. Schäfer, A. R. Vilenskiy, L. Nyström, A. A. Kishk, and M. V. Ivashina, "Low-profile, K-/Ka-band $\pm 60^\circ$ 2-D-scanning dual-polarized patch antenna array on a triangular lattice for SATCOM-on-the-move applications," submitted for publication.